Modelling tritium adsorption and desorption from tungsten dust particles with a surface kinetic model

Etienne A Hodille, M Payet, V Marascu, S Peillon, J Mougenot, Y Ferro, Rémi Delaporte-Mathurin, F Leblond, E Bernard, C Grisolia

Postprint of article accpeted for publication in Nuclear Fusion as:
https://doi.org/10.1088/1741-4326/ac0f37

Modelling tritium adsorption and desorption from tungsten dust particles with a surface kinetic model

E A Hodille[1], M Payet[1,2] V Marascu[2,3], S Peillon[4], J Mougenot[5], Y Ferro[6] , R. Delaporte-Mathurin[1,5], F. Leblond[1], E Bernard[1], C. Grisolia[1]

[1] CEA, IRFM, F-13108 Saint Paul Lez Durance, France
[2] Université Paris-Saclay, CEA, INRAE, DMTS, SCBM, F-91191 Gif-sur-Yvette, France
[3] National Institute for Lasers, Plasma and Radiation Physics, P.O. Box M G-36, 077125 Magurele, Romania
[4] IRSN, PSN-RES, SCA Gif-sur-Yvette 91192, France
[5] Université Sorbonne Paris Nord, Laboratoire des Sciences des Procédés et des Matériaux, LSPM, CNRS, UPR 3407, F-93430 Villetaneuse, France
[6] Aix-Marseille Université-CNRS, PIIM UMR 7345, 13397 Marseille, France

E-mail: `etienne.hodille@gmail.com`

Abstract. A kinetic surface model is presented and used to explain the loading and desorption kinetics of tritium retained in micrometre-sized tungsten (W) dust particles. The model describes the sticking of hydrogen isotopes from the gas phase to W surfaces and the desorption from W surfaces. The initial sticking coefficient is set to one and independent of the temperature. The activation energy for desorption depends on the hydrogen coverage of the surface and is parametrised with density functional theory (DFT) calculations for W(100), W(110) and W(111) surfaces. The DFT-parametrised model is successfully compared to experimental results showing that the amount of measured tritium as well as the desorption kinetic can be modelled with only tritium adsorbed on the surface of W dust particles. Then, the model is used to explore possible scenarios to remove the tritium from the W surfaces by exposing the tritiated surfaces to either deuterium and hydrogen. The simulations suggest that it can be possible to remove all the tritium trapped on the W surfaces even at room temperature as soon as the hydrogen or deuterium pressure is higher than the tritium pressure. This gives opportunity to build tritium removal scenarios for ITER.

Keywords: Tritium, tungsten, dust, surface, isotopic exchange

1. Introduction

The plasma wall interactions in tokamaks will lead to formation of different sizes and shapes of dust particles. In ITER, both Tungsten (W) and Beryllium (Be) dust are expected [1] in the 100 kg range. In DEMO, where W is the main plasma facing material, W dust are expected in the 1000 kg/year range [2].

These dust particles may be problematic for the safe operation of a tokamak as they can be a high reservoir of tritium, even though the mass of dust is below the 1000 kg safety limit [3]. Indeed, it has been shown that W dust can be loaded with up to 10 GBq/g of tritium for nanometre-sized dust [4, 5, 6] and micrometre-sized dust could be loaded with up to 300 MBq/g [7]. In addition, depending on the size and tritium distribution in the dust, as tritium decays, the dust particles may be electrically charged [3, 7] even if they are not exposed to the plasma (for instance below the divertor where most of the produced dust are expected to be [1]). It would influence their transport in the plasma and possibly creating an additional source of W impurities if they are mobilised by their electric charge when the magnets are turned on. Thus, the study of tritium loading in dust is one of the critical issue for tokamak operations as a significant quantity of dust is expected during ITER operation as calculated by Shimada *et al* [1].

In previous studies [7], micrometre-sized dust has been loaded with tritium following the procedure developed in [4]. After reduction of the oxide layer under 10^5 Pa hydrogen at 743 K, the dust is sealed in a vial under a tritium pressure at 300 K. The vial is then heated up to 743 K so the tritium pressure is 1.1×10^5 Pa for several hours and quenched to liquid nitrogen before being heated up to room temperature. Then, the vial is unsealed and the tritium desorbing from the dust is detected. The final amount of tritium remaining in the dust after hundreds of hours of room temperature desorption is detected after the full dissolution of the dust. Peillon *et al* [7] observe that the tritium content in micrometres-sized dust at the end of the procedure is in the range of 100 MBq/g while about the same amount is desorbed in hundreds of hours at room temperature. In order to explain these experimental observations, we present a surface kinetic model presented in [8, 9]. This kinetic surface model has already been presented as a boundary condition for model of diffusion and trapping of hydrogen in bulk W [10, 11]. In this work, the model is extended to be able to handle several hydrogen isotopes and it is parametrised with coverage dependent desorption energies coming from Density Functional Theory (DFT) calculations [12, 13]. After a successful simulation of the experimental results, different scenarios are considered involving isotopic exchange. They can be used to design further experimental scenarios to validate the model and suggest ways to remove the tritium from W dust.

2. Description of the model

Here, we simulate tritium loading and desorption from W dust particles reported in [7] in which several dust batches are considered. We focus the simulations on the dust batch for which the tritium loading experiment has been repeated and confirmed. This batch (labelled AF5 in [7]) is characterised by the number distribution $f(r)$ given in figure 1, such that $f(r)dr$ gives the number fraction of particles with a radius between r and $r + dr$. Appendix A explains how to calculate the tritium massic activity using this particle-size distribution.

2.1. Tritium trapping on the surface and in the bulk

For any particle sizes, we consider two extreme cases: (i) all the tritium is homogeneously distributed in the bulk with a concentration c_T (m^{-3}) and (ii) all the tritium is trapped on the surface of the dust particle with a concentration $c_\mathrm{T,s}$ (m^{-2})

Using appendix A, in the case (i), the massic activity is:

$$a_\mathrm{m} = \frac{\omega}{d_\mathrm{W}} c_\mathrm{T} \tag{1}$$

where the W density is $d_\mathrm{W} = 19.3 \times 10^6$ gm^{-3} and $\omega = 360 \times 10^{12} A_\mathrm{T}/N_\mathrm{A}$ is employed to convert a quantity of tritium atoms into a tritium activity, with $N_\mathrm{A} = 6.022 \times 10^{23}$ mol^{-1} the Avogadro number and $A_\mathrm{T} = 3$ g/mol the atomic mass of tritium. The massic activity does not depend on the size of the particles and depends only on how much tritium can be loaded in bulk W at the loading conditions, i.e. the tritium solubility in W.

In the case (ii), the massic activity is:

$$a_\mathrm{m} = \omega c_\mathrm{T,s} \mathrm{SSA} \tag{2}$$

where SSA $= \frac{\int_0^{+\infty} f(r)S(r)dr}{d_W \int_0^{+\infty} f(r)V(r)dr}$ is the specific surface area (m^2g^{-1}) [14] which gives the amount of surface in contact with the gas per mass (or volume) of dust. The massic activity is proportional to the amount of tritium that is possible to load on a W surface and to the size of the specific surface area, i.e. the size of the particles (assuming they are spherical).

Peillon *et al* [7] compiled the data of tritium trapped in dust from different studies, including their own, from sub-micrometre-sized dust [4, 6] to micrometre-sized dust. A clear increase of the activity of tritium with the specific surface area is reported supporting case (ii) and a retention of tritium dominated by surface effects. Thus, we only consider the surface effects in this work. The possible contribution of the tritium in the bulk is discussed later on and in appendix B.

2.2. Model of adsorption and desorption of hydrogen on W surfaces

We consider that the surface of the W dust can be exposed to H_2, D_2 and T_2 at a given temperature T_g (K) and at a given partial pressure $p_{X_2, X\in\{H,D,T\}}$ (Pa). The partial pressure p_{X_2} turns into a flux of molecules Γ_{X_2} (in $m^{-2}s^{-1}$) on the surface:

$$\Gamma_{X_2} = \frac{p_{X_2}}{\sqrt{2\pi m_X k_B T_g}} \tag{3}$$

with m_X (kg) the mass of the molecules considered and k_B the Boltzmann constant.

On the W surface, the concentration of adsorption sites is n_{surf} (m^{-2}):

$$n_{surf} = n_s \rho_W^{2/3} \tag{4}$$

where ρ_W is the tungsten atomic density: there are 2 W atoms per cube of side $a = 316$ pm in bcc W so $\rho_W = 2/a^3 = 6.33 \times 10^{28}$ m^{-3}. Thus, n_s ~~can be~~ is understood as the number of adsorption site per W atom on an average W surface.

The concentration of adsorbed hydrogen isotopes of type X is $c_{surf,X}$ (m^{-2}). The surface coverage of the species X if defined as:

$$\theta_X = \frac{c_{surf,X}}{n_{surf}}. \tag{5}$$

Similarly, the normalised molecule flux of species X, γ_{X_2} (s^{-1}), impinging the surface is:

$$\gamma_{X_2} = \frac{\Gamma_{X_2}}{n_{surf}} \tag{6}$$

Considering that the surface is exposed to H_2, D_2 and T_2, and that the hydrogen isotopes can be outgassed via a second order process, the evolution of the system is described by the following set of equations derived from [8] and [9]:

$$\frac{d\theta_H}{dt} = 2\gamma_{H_2} s_{H_2}(T_g)(1-\theta_{tot})^2 - 2\nu_{des}^{H+H}(T)\theta_H^2 - \nu_{des}^{H+D}(T)\theta_H\theta_D - \nu_{des}^{H+T}(T)\theta_H\theta_T \tag{7}$$

$$\frac{d\theta_D}{dt} = 2\gamma_{D_2} s_{D_2}(T_g)(1-\theta_{tot})^2 - 2\nu_{des}^{D+D}(T)\theta_D^2 - \nu_{des}^{H+D}(T)\theta_H\theta_D - \nu_{des}^{D+T}(T)\theta_D\theta_T \tag{8}$$

$$\frac{d\theta_T}{dt} = 2\gamma_{T_2} s_{T_2}(T_g)(1-\theta_{tot})^2 - 2\nu_{des}^{T+T}(T)\theta_T^2 - \nu_{des}^{H+T}(T)\theta_H\theta_T - \nu_{des}^{D+T}(T)\theta_D\theta_T \tag{9}$$

where $\theta_{tot} = \theta_H + \theta_D + \theta_T$, the total hydrogen isotope coverage of the surface, $s_{X_2}(T_g)$ (dimensionless) the initial sticking probability of the X_2 molecule possibly dependent on the temperature of the gas T_g and $\nu_{des}^{X+Y}(T)$ the desorption rate constant (s^{-1}) for the elementary second order desorption reaction $X + Y \rightarrow XY$ that depends on the temperature of the W surface T.

The sticking of X_2 on the surface is characterised by the equation $X_2(g) + 2S_{free} \rightarrow 2X_{surf}$, where S_{free} is a free adsorption site on the surface. Assuming this is an elementary process, the speed of this reaction is proportional to the square of the concentration of S_{free}, i.e. $(1-\theta)^2$.

The desorption rate constant is expressed as:

$$\nu_{des}^{X+Y}(T) = \nu_0^{X+Y} \exp\left(-\frac{E_{des}^{X+Y}(\theta_{tot})}{k_B T}\right) \tag{10}$$

where ν_0^{X+Y} is the pre-exponential factor (s^{-1}) and E_{des}^{X+Y} (eV) is the activation barrier for the desorption of the XY molecule, that can depend on the total coverage of the surface as shown by density functional theory (DFT) calculations [15, 12, 13, 16] and experimental results [17, 18]. The mass difference of the hydrogen isotopes is taken into account in the pre-exponential factor as:

$$\nu_0^{X+Y} = \frac{\nu_0}{\sqrt{1/2\,(A_X + A_Y)}} \tag{11}$$

where A_X is the atomic mass of the hydrogen isotope X and $\nu_0 = 10^{13}$ s^{-1}.

This model is solved using the SciPy's [19, 20] optimize.fsolve function. All plots in this work were generated with Matplotlib [21].

3. Simulation of tritium loading and desorption experiment

In this section, we will consider that there is only one hydrogen isotope (tritium) reacting with the surface: only equation 9 is solved to calculate θ_T.

We simulate the adsorption of tritium on the surface of a dust batch characterised by the bimodal

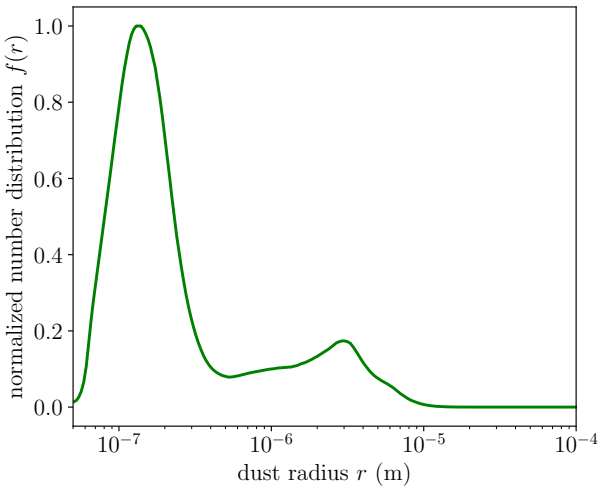

Figure 1: Normalized number distribution $f(r)$ for the AF5 batch.

number distribution given in figure 1. The first mode contains the majority of particles with radius around 100 nm. The second mode indicates the presence of a rather important population of micrometre-sized particles in this powder. It follows that the mass distribution exhibits a mediam radius of 5.75 μm [7] which is the range of sizes that contributes the most to the massic activity.

In these experiments, prior to the tritium loading, the native oxide layer on the W particles is reduced at 743 K under a hydrogen atmosphere. One can consider that during the tritium loading, the tritium gas is in contact with a metallic surface. The initial sticking coefficient of H has been measured for perfect W(100). It varies between 0.5-0.7 [22] and is independent of temperature [23]. In addition, DFT calculations show that the activation energy for the dissociation of H_2 on W(100), W(110) and W(111) is close to zero [12, 13, 13]. Thus, in these simulations, the sticking coefficient is also assumed to be independent of the temperature and set to unity.

3.1. Coverage dependent desorption energy

DFT calculations of H on W surface [15, 12, 13, 16] and experimental results [17, 18] suggest that the activation energy E_{des} to desorb from the surface depends on the coverage. Such a model has already been considered in the MISTRAL model for tritium transport in breeding blankets lithium-based ceramics [24].

In previous simulation studies, we took this into account by considering a continuous function $E_{\text{des}}(\theta)$ with the following form [11]:

$$E_{\text{des}}(\theta) = E_0 + \Delta E \frac{1}{1+\exp\left(\frac{\theta-a}{b}\right)} \tag{12}$$

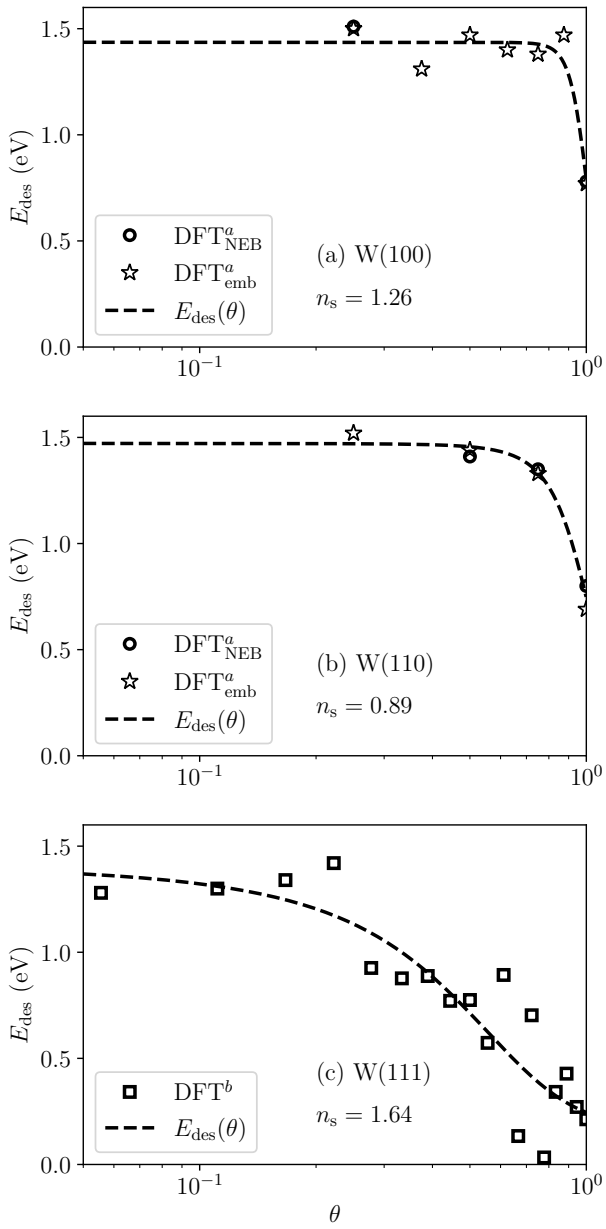

Figure 2: Evolution of desorption energies E_{des} with the relative coverage θ for W(100) (a), W(110) (b) and W(111) (c). The open symbols represent the DFT data from [12]^a (a), (b) and from [13]^b (c). The dashed line are the fit given by SciPy optimize.curve_fit function. For the DFT data from [12], the desorption energies are calculated with two methods: Nudge Elastic Band (NEB) or energy difference between adsorption state and gas state (emb). For the DFT data from [13], only the energy difference between adsorption state and gas state are reported.

Table 1: Lists of parameters that are used to fit the DFT data and give the continuous function $E_{\text{des}}(\theta)$ for W(100), W(110) and W(111).

	$W(100)$	$W(110)$	$W(111)$
E_0 (eV)	0.142	0.019	0.178
ΔE (eV)	1.294	1.453	1.389
a	1.000	1.000	0.407
b	0.050	0.111	0.199

To initialise our model, we used the desorption energies calculated by DFT for W(100) and W(110) [15, 12] and for W(111) [13].

According to Piazza *et al* [15], the H saturation happens for 2 H/W on W(100) and 1 H/W on W(110) when exposed to gas. Thus, the parameter n_s is 1.26 for W(100) and 0.89 for W(110). The calculated activation energy barriers are taken from [12] and shown in figure 2(a) and (b).

For W(111), Bergstrom *et al* [13] calculated that up to 4.5 H/W, it is more favorable to adsorb 1 additional H: it is set as the saturation limit for this surface and $n_s = 1.64$ for W(111). Bergstrom *et al* reported the consecutive adsorption energy as a function of coverage, i.e. for a number N of adsorbed hydrogen H_s, the energy gain of the reaction $NH_s + {}^1/_2H_2 \rightarrow (N+1)H_s$. The desorption energy is the energy loss of the reaction $(N+2)H_s \rightarrow H_2 + NH_s$. As there is no activation energy for the dissociation of H_2 on W(111) [13] and considering that N is large enough so $N+2 \approx N+1 \approx N$, E_{des} is approximated to twice the energy calculated by Bergstrom (=consecutive adsorption energy). This is the value shown in figure 2(c).

From these discrete DFT data, a non-linear least square regression fit is applied using SciPy's [19, 20] optimize.curve_fit module and the expression 12. Figure 2 shows the evolution of E_{des} with the relative coverage θ for W(100) (a), W(110) (b) and W(111) (c) as well as the continuous function that will be used in the kinetic simulations. For each surface, the list L of the 4 parameters needed for the expression 12, is reported in table 1.

The DFT calculations show similar trends for the different surfaces. The desorption energy from the bare surface is about 1.4-1.5 eV. For W(110) and W(100) the desorption energy for saturated surface is ≈0.7-0.8 eV. On the contrary, the desorption energy at saturation is ≈ 0.3 eV on W(111). The saturation of such a surface would be almost impossible except at very low temperature: Tamm and Schmidt report a coverage above 4 H/W on W(111) at 78 K [17]. In addition, Tamm and Schmidt report very low temperature peaks after flash desorption experiment on W(111) which are abstent for W(110) and W(100) [17].

3.2. Scenario of the simulations

The details about the experimental procedure to load W dust with tritium gas is described in [4, 5, 6, 7] and we summarized it here to define our simulation scenario. After the reduction of the oxide layer, the dust are put in a sealed vial under an T_2 atmosphere so that at 743 K, the tritium pressure is $1.1{\times}10^5$ Pa. After being exposed to this atmosphere for 2 hours, the sealed vial is put in liquid nitrogen to freeze the processes. Then the vial is heated up to room temperature, the vial is unsealed and the tritium desorption measurements start under a carrier gas. This allows us to define a scenario for our simulations of tritium loading/desorption in 5 steps:

(i) Exposure to T_2 with $p_{T_2} = 1.1 \times 10^5$ Pa and $T = 743$ K.

(ii) Thermal quench from 743 K to 77 K in 10 seconds and p_{T_2} goes down to $1{\times}10^4$ Pa.

(iii) Increase from 77 K to 300 K in 100 seconds and p_{T_2} goes up to $4{\times}10^4$ Pa.

(iv) At 300 K, the vial is unsealed and the carrier gas starts flowing on the dust: the partial pressure of T_2 drops to 0 Pa in 10 s and stay equal to zero for another 90 seconds.

(v) At 300 K, the partial pressure of T_2 is maintained to 0 by the carrier gas, allowing the tritium to freely desorbs from the dust.

Since the surfaces are only exposed to tritium, only equation 9 is solved for each steps.

3.3. Simulation results

For all surfaces, the tritium coverage θ_T is calculated with the desorption energies given in figure 2. The evolution of both tritium coverage θ_T and desorption energy E_{des} during the 5 steps of the simulation scenario are reported in figure 3.

For W(110) and W(100) surfaces, the evolution of tritium coverage from step (i) to step (v) is fairly similar thanks to the similar evolution of desorption energy with coverage (see figure 2). In particular, the steady-state is reached within 10^{-7} s during step (i). Indeed, at a pressure of $1.1{\times}10^5$ Pa, the flux of molecules on the surface is $\approx 10^{28}$ m^{-2}s^{-1} leading to a fast sticking of tritium atoms. The tritium coverage at steady-state is ≈ 0.9 leading to $E_{\text{des}} \approx 1.0$ eV. With such a high coverage, there is not enough adsorption sites available for the sitcking flux $\propto (1-\theta)^2$ to

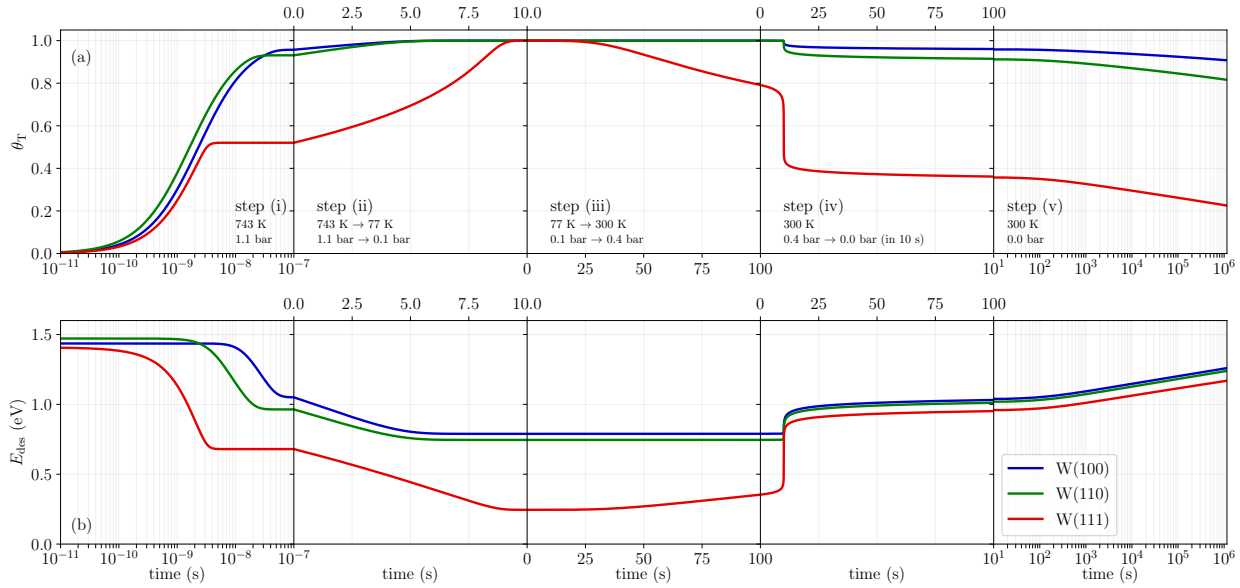

Figure 3: Evolution of the tritium coverage θ_T (a) and the desorption energy E_{des} (b) during the 5 steps of the scenario for the 4 considered evolution of $E_{des}(\theta)$.

compensate the desorption flux $\propto \theta^2$: it prevents the desorption energy to decrease further.

For W(111) in the first step, the steady-state is also quickly reached but the equilibrium tritium coverage is lower (≈ 0.5). Hence, the value of $(1-\theta)^2$ allows sticking at lower value of E_{des} than for W(100) and W(111). For the remaining steps, the tritium coverage experience much more variations than for W(100) and W(110). Indeed, the desorption energy for W(111) varies on a bigger amplitude with smoother variations (see the parameter b on table 1).

During the step (v), which will be compared to the experimental desorption data, the tritium coverage on all surfaces decreases. The loss of coverage $\Delta\theta$ leads to an increase of the desorption energy ΔE_{des}. The initial coverage θ_i at the beginning of this step, the relative coverage loss $\frac{\Delta\theta}{\theta_i}$, the initial desorption energy $E_{des,i}$ and the increase of the desorption energy ΔE_{des} are reported in table 2. For all surfaces, the desorption energy at the beginning of step (v) is ≈ 1.0 eV and the gain in desorption energy ΔE_{des} is the same $\approx 0.21-0.22$ eV. However, the relative coverage loss is 5% for W(100), 10% for W(110) and 37% for W(111): the smother the transition of E_{des} is, the bigger the coverage loss can be.

3.4. Comparison with experimental results

For each surface W(ijk), the evolution of the tritium coverage during step (v) can be converted in a tritium activity $a_{W(ijk)}$ with the size distribution of the dust (figure 1). The fraction of the dust covered by W(ijk) is $0 \leq s_{W(ijk)} \leq 1$ with $\sum_{W(ijk)} s_{W(ijk)} = 1$. We assume that the contribution of the tritium activity of one surface is independent of the others. Thus, the total tritium activity is calculated as the linear combination of activity for each surface weighted by its fraction:

$$a_{tot} = \sum_{W(ijk)} s_{W(ijk)} a_{W(ijk)}. \quad (13)$$

We assume that the dust surface contains only the three surfaces W(110), W(100) and W(111). In theory, there can be much more surface orientations but we have coverage dependent desorption energy only for those ones. Plus, these 3 surfaces seems to be a good pictures of the different possible behaviour of H desorption from clean W surfaces: E_{des} goes from 1.4 eV (for bare surface) to low desorption energy (at saturation) with either a sharp transition (W(100) and W(110)) or a smooth transition (W(111)).

Table 2: Initial coverage θ_i, the relative coverage loss $\frac{\Delta\theta}{\theta_i}$, initial desorption $E_{des,i}$ and modification of desorption energy ΔE_{des} during step (v) for the different surfaces considered here.

	θ_i	$\Delta\theta/\theta_i$	$E_{des,i}$	ΔE_{des}
W(100)	0.960	0.054	1.034 eV	0.224 eV
W(110)	0.913	0.107	1.016 eV	0.224 eV
W(111)	0.359	0.37	0.956 eV	0.213 eV

Considering these 3 surfaces, one needs three fractions $s_{\mathrm{W}(110)}$, $s_{\mathrm{W}(100)}$ and $s_{\mathrm{W}(111)}$. Since, there is $\sum_{\mathrm{W}(ijk)} s_{\mathrm{W}(ijk)} = 1$, fixing two of these fractions is enough. The parameter space can be reduced to two:

- $s_{\mathrm{W}(111)}$, the fraction of W(111) surface,
- $s_{\mathrm{W}(110)}$, the fraction of W(110) surface.

Introducing $x_{\mathrm{W}(110)} = {}^{s_{\mathrm{W}(110)}}/_{1 - s_{\mathrm{W}(111)}}$ as the fraction of W(110) surface in the remaining surfaces, one calculate the fraction of W(100) as:

$$s_{\mathrm{W}(100)} = (1 - x_{\mathrm{W}(110)})(1 - s_{\mathrm{W}(111)}). \tag{14}$$

Considering a set of parameter $P = (s_{\mathrm{W}(111)}, x_{\mathrm{W}(110)})$, one obtains a simulated tritium activity $a_{\mathrm{sim}}(t, P)$ with equation 13. To quantify the agreement between the activity measured experimentally $a_{\mathrm{exp}}(t_i)$ and this simulated activity, we use the following cost function:

$$f_{\mathrm{c},2}(P) = \sum_i \left(\frac{a_{\mathrm{exp}}(t_i) - a_{\mathrm{sim}}(t_i, P)}{\delta_i} \right)^2 \tag{15}$$

with δ_i the uncertainty on the experimental measurement which is estimated to be 10%. Figure 4(a) shows the evolution of the cost function in the plane $(x_{\mathrm{W}(110)}, s_{\mathrm{W}(111)})$. It is focused on $0.75 \leq s_{\mathrm{W}(111)} \leq 1.00$ which is the region where is its minimum. For a given value of $x_{\mathrm{W}(110)}$, there is a single minimum of $f_{\mathrm{c},2}$ forming a valley of minimums in the whole plane. Figure 4(b) shows the comparison between the experimental data and the best simulated tritium activity for three values of $x_{\mathrm{W}(110)}$ (0.0, 0.5 and 1.0). It also presents the simulated tritium activity in the corner of the parameter space, i.e. with only one surface orientation. The linear combination given by equation 13 spans between these simulated activities.

According to figure 4, in order to get a good comparison between simulations and experiments, one needs a major contribution of W(111) (≥ 0.8). Indeed, in experiments, the tritium loss is between 26 % and 50 % (considering the experimental error bars while it is 37% for W(111) (table 2). However, if one consider only W(111), the simulated at the beginning of step (v) is too low (0.406 GBq/g) compared to the experimental one (0.469 GBq/g). Thus, a fraction of other surfaces is needed to act as an offset to the total tritium activity. It should be noted that this offset could as well come from a constant bulk contribution and the trapping parameters could be estimated using the model given in appendix B.

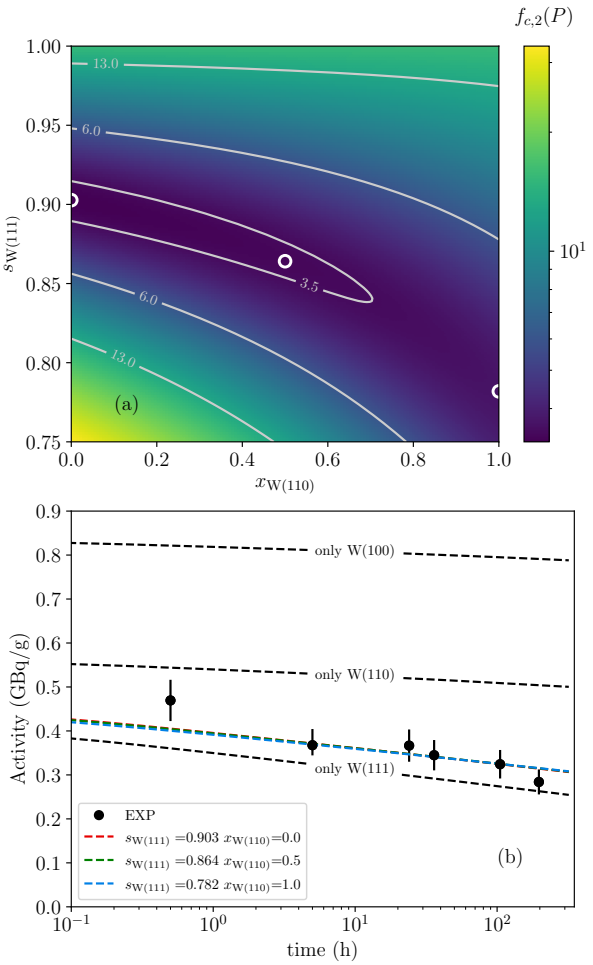

Figure 4: For batch AF5, (a) Cost function $f_{\mathrm{c},2}(P)$ in the plane $(x_{\mathrm{W}(110)}, s_{\mathrm{W}(111)})$ (the color bar is in logarithmic scale). (b) comparison between the experimental tritium activity and the simulated tritium activity for three different set of parameters, represented by white circle in (a) which gives an good fit of the experimental data. In addition, the simulated tritium activities in the corner of the parameter space (labeled *only W(1xy)*) are shown. There is a one-hour uncertainty on the first measurement point represented in a shadowed area.

4. Exposure to a mixed isotope gas

In the previous section, we have shown that it is possible to simulate trapping and release of tritium from W dust considering only the surface of the dust particles. Here, we investigate a possible way to retrieve the tritium trapped on the surface using isotope exchange by exposing the dust to H_2 or D_2. Isotopic exchange on the surface has already been explored experimentally for surfaces of polycristaline W exposed to D atom [8, 25] and for W(100) surface exposed to very low gas pressure [26]. Here, we consider different sets of conditions from ($1{\times}10^4$ Pa, 300 K) to (1 Pa, 373 K). It could help design procedure for tritium removal from dust particles either once they are removed from the vessel or directly during the exploitation of a tokamak.

4.1. High pressure isotopic exchange

First, we consider the possibility to extract the tritium from the W surfaces at 300 K by exposing them to H_2 with a pressure of $1{\times}10^4$ Pa. The initial tritium coverage is set to the initial tritium coverage in table 2 (corresponding to the beginning of step (v)). The pressure of H_2 is directly set to be $1{\times}10^4$ Pa so we get a step response of the tritiated surface. In theory, desorption of T_2 and HT should increase the partial pressure of these respective gases, creating another source of molecules. However, in the case of a small amount of dust in a large volume of gas, we did not simulate the re-sticking of T through dissociation of HT and T_2.

Equation 7 and 9 are solved in the simulations for the 3 considered surfaces and figure 5 shows the evolution of tritium and hydrogen coverage (a), the evolution of the outgassing fluxes from the surface as H_2, T_2 and HT (b) and the evolution of the desorption energy (c). The outgassing fluxes of the molecule XY in $m^{-2}s^{-1}$ is $\phi_{des}^{XY} = n_{surf}\nu_{des}^{X+Y}(T)\theta_X\theta_Y$. For all surfaces, the tritium is completely recovered at 300 K under $1{\times}10^4$ Pa of H_2 after less than 20 seconds. It occurs after about 10 seconds of exposure on W(100), 2 secondes on W(110) and 10^{-6} seconds on W(111). The kinetics of tritium recovery depends strongly on the desorption energy during the process which depends on the total coverage $\theta_{tot} = \theta_H + \theta_T$ at equilibrium.

For W(100) and W(110), θ_{tot} reaches unity quickly and the desorption energy is ≈0.7-0.8 eV (figure 5(c)). With such coverage and desorption energy, the outgassing flux of tritium as T_2 or HT remains high ≈10^{18}-10^{19} $m^{-2}s^{-1}$ (figure 5(b)) which represents the content of 0.1-1 ML (monolayer) desorbing per seconds (figure 5 (b)).

For W(111), the recovery is much faster because the desorption energies reaches much lower value. When the pressure of hydrogen is triggered, E_{des} decreases to 0.35 eV (figure 5 (c)). It represents a outgassing flux of tritium in T_2 and HT of $3{\times} \approx 10^{25}$ $m^{-2}s^{-1}$, depleting all the tritium present on the surface in 10^{-6} s.

4.2. Toward tokamak conditions

4.2.1. Tritium loading During operations of tokamaks like Tore Supra, ASEDX-Upgrade or JET, the background pressure is in the range of 10^{-5} - 10^{-6} Pa [27, 28, 29, 30]. At the end of the plasma, as the hydrogen isotopes recombines (and possibly desorbs from the wall), the pressure of hydrogen isotopes molecules increases and can reach few Pa. Considering that ITER will operate, in its nuclear phase, with an equal mixture of deuterium and tritium, we consider that the pressure of tritium, p_{T_2}, and deuterium, p_{D_2}, are equal. Thus, we define here a simple model scenario to simulate tritium capture during the recombination of the plasma:

(i) for 45 seconds, $p_{D_2} = p_{T_2} = 10^{-6}$ Pa,

(ii) in 5 seconds, both pressures increase linearly up to 1 Pa,

(iii) in 5 seconds, both pressures decreases linearly back to 10^{-6} Pa,

(iv) $p_{D_2} = p_{T_2} = 10^{-6}$ Pa for 45 more seconds.

We choose the lower limit for the partial pressure of T_2 and D_2 as it is the case for which the flux of molecules to the surface will be the lowest. It gives a lower limit for the amount of tritium trapped on the surface. We consider dust particles below the divertor. Thus, they are not heated by the plasma and their temperature remains equal to 373 K for the duration of the simulation. Initially, the dust are considered free of any adsorbed hydrogen isotopes (bare surface).

Equation 8 and 9 are solved with the pressure evolution shown on figure 6(a) and figure 6 (b)-(d) show the evolution of the tritium coverage θ_T, deuterium coverage θ_D and total coverage $\theta_{tot} = \theta_T + \theta_D$. For all surfaces, the tritium coverage is slightly below the deuterium coverage because of the isotope mass effect (equation 3 and 11).

The simulations show that even a small tritium pressure of 10^{-6} Pa is enough to load significantly the surface of the dust particles with tritium. The increase of the pressure increases both tritium and deuterium coverage up to the saturation of the surface. Once the pressures decrease back to 10^{-6} Pa, both coverage decreases toward the hydrogen isotope coverage at equilibrium for a pressure of 10^{-6} Pa at 373 K. As Predicted by thermodynamoc model parametrized with DFT data [16, 31], this equilibrium coverage is close to 1 for W(100) and W(110) in the temperature and pressure conditions used here. Considering the parametrisation of the section 3, the tritium activity would reach 300 MBq/g at the pressure peak and 200 MBq/g at the end of the scenario. Thus, even at a T_2 partial pressure as low as the lower limit of the background pressures expected in a tokamak, the tritium can be easily captured up to saturation of the surface. In simulations with a higher background pressure of 10^{-4} Pa (for bigger machine like ITER), the tritium coverage follows the same trends as presented in figure 6. The only difference is an increase of the final tritium coverage of 20% for W(111), 4% for W(110) and 2% for W(100) when compared to the simulation with a background pressure of 10^{-6} Pa.

4.2.2. Tritium recovery Now that the surface of the dust are loaded with a mixture of D and T, we

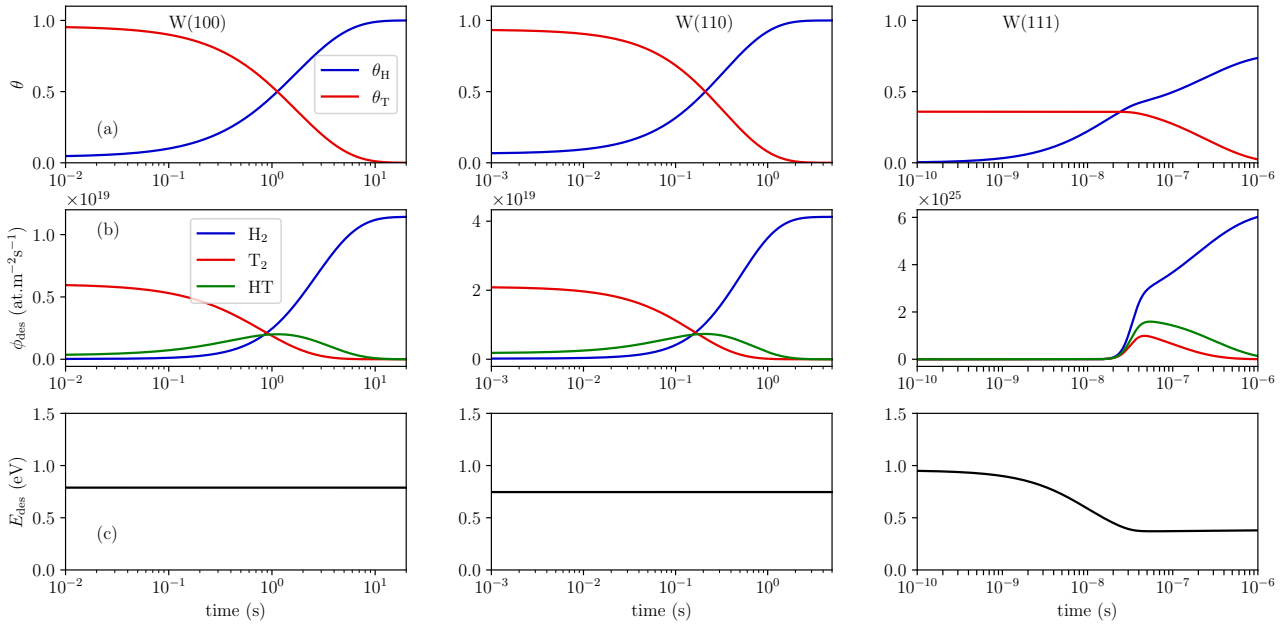

Figure 5: Tritium and hydrogen coverage (a), T_2, H_2 and HT desorbing flux (b) and desorption energy (c) for W(100), W(110) and W(111) during an exposure at $1{\times}10^4$ Pa of H_2 at 300 K with an initial tritium coverage in table 2 (beginning of step (v)).

investigate a way to recover this tritium using isotopic exchange following the scenario:

(i) increase of p_{D_2} to 1 Pa in 5 seconds and p_{T_2} remains equal to 10^{-6} Pa,

(ii) stabilisation of deuterium pressure to 1 Pa for 10 seconds,

(iii) decrease of p_{D_2} either back to 10^{-6} Pa or to 10^{-5} Pa in 5 seconds

(iv) constant deuterium and tritium pressure up to 1000 s.

The temperature remains constant equal to 373 K and the initial coverage of the simulations are the one obtained at the end of the previous scenario (figure 6).

Equation 8 and 9 are solved with the pressure evolution shown on figure 7(a) and figure 7 (b)-(d) report the evolution of θ_T and θ_D for the different surfaces. For all surfaces, as soon as p_{D_2} becomes higher than p_{T_2}, the tritium coverage decreases quickly. To quantify the speed to exchange the tritium by deuterium, we report in table 3 the time $t_{95\%}$ and pressure $p_{D_2,95\%}$ when $\theta_D \geq 0.95\theta_{tot}$ in the first stage to the scenario. The isotopic exchange is completed at 95% in less that 5 seconds in all cases (table 3): all the tritium is recovered before reaching the deuterium pressure plateau at 1 Pa. It is especially fast for the W(111) because its low desorption energies. Changing the increase of deuterium pressure from 1 Pa to 0.1 Pa only change the kinetics of the isotopic exchange without changing its efficiency after 20 seconds.

Table 3: Value of time ($t_{95\%}$) and deuterium pressure ($p_{D_2,95\%}$) at which the deuterium coverage is 95% of the total coverage during the pressure ramp up. The T_2 pressure is kept constant equal to 10^{-6} Pa and the temperature is 373 K.

	$t_{95\%}$	$p_{D_2,95\%}$
W(100)	3.79 s	0.76 Pa
W(110)	1.44 s	0.29 Pa
W(111)	0.12 s	0.02 Pa

When the deuterium pressure decreases and reaches 10^{-6} Pa, θ_T increases in order to reach the equilibrium that existed before the isotopic exchange step. On W(100) and W(110), the kinetic is slow and after 980 seconds, deuterium stays the main adsorbed isotopes. However, on W(111), the equilibrium is reach in about 200 seconds and $\theta_T \approx \theta_D$. When the deuterium pressure at the end of the scenario is one order of magnitude above the tritium pressure, (dashed line in figure 7) the deuterium stays the main adsorbed isotopes with $\theta_T \approx 0.1\theta_D$. Thus, to make the isotopic exchange on the surface efficient, one need to keep a tritium pressure lower than the deuterium pressure.

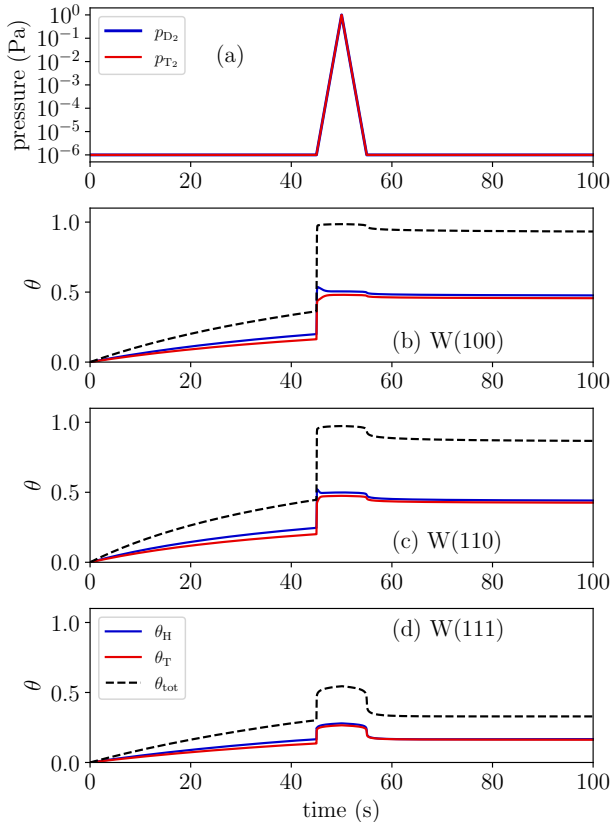

Figure 6: (a) evolution of the D_2 and T_2 pressure during a possible increase of the partial pressure in the tokamak vessel due to plasma recombination: the background pressure of T_2 and D_2 is 10^{-6} Pa and it increases to 1 Pa. (b), (c) and (d) give the evolution of the tritium coverage θ_T, deuterium coverage θ_D and total coverage θ_{tot} during the scenario for W(100), W(110) and W(111). The temperature in these simulations is 373 K.

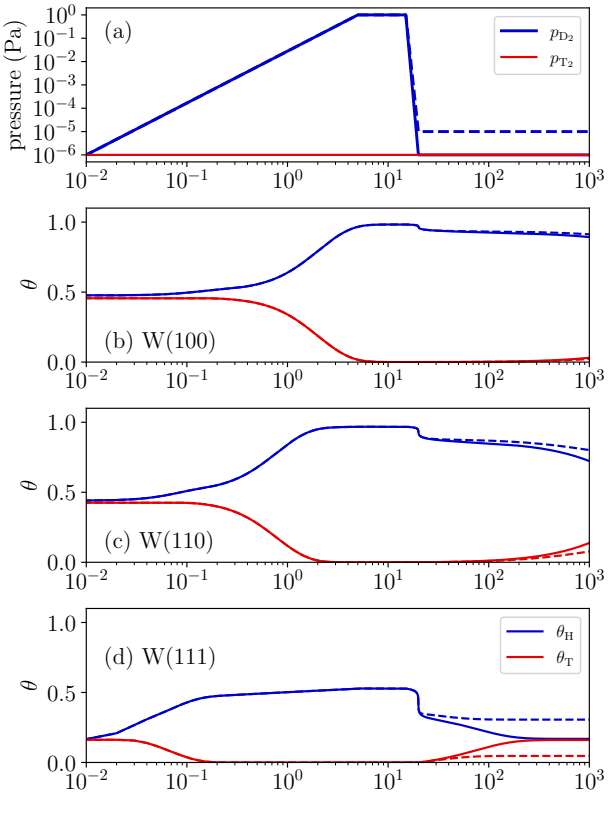

Figure 7: (a) evolution of the D_2 and T_2 pressure during an in-vessel isotopic exchange scenario. (b), (c), (d) give the evolution of the tritium coverage θ_T and deuterium coverage θ_D during the scenario for W(100), W(110) and W(111). For the last part of the scenario, the solid line represent the case when p_{D_2} decreases to 10^{-6} Pa and the dashed line when it decreases to 10^{-5} Pa. The temperature in these simulations is 373 K.

5. Discussion

5.1. impact of the bulk of the dust particles

In section 3, the contribution of the tritium activity on W(110) and W(100) is used as an offset to match the total tritium activity measured in the experiment. This offset could as well come from a bulk contribution. The bulk of each dust particles is populated with defects that can trap tritium atoms. These traps are characterised by the couple $(E_{dt,i},n_i)$ which are the detrapping energy $E_{dt,i}$ (eV) and the trap concentration n_i (atomic fraction). The bulk contribution can be calculated using appendix B. Using the traps determined for annealed poly crystalline W [32], i.e. with detrapping energy below 1.00 eV, one obtain a bulk contribution equal to 0.027 MBq/g. However, the studied dust particles are not annealed poly crystalline W and some traps with high detrapping energy created during the dust production may be present in the bulk of the dust particles. Using the model in appendix B, it is calculated that the concentration of tritium in the bulk should be around 10^{-4} atomic fraction ($\approx 6 \times 10^{24}$ m^{-3}) to reach a massic activity of 100 MBq/g (as in the experiment) in the bulk. Such a large quantity of tritium, with a low solubility of interstitial hydrogen, requires a high concentration of very deep defects (>1.5 eV of detrapping energy, i.e. vacancy-type defects [33, 34]) coming from the dust production. Note that the bulk contribution, in the assumption of a homogeneous distribution of tritium, does not depend on the surface specific area (section 2.1). Thus, to retrieve the dependence of tritium inventory with the surface specific area, higher concentrations of traps have to be assumed for smaller dust. A better assessment of the microstructure of the dust particles prior to the tritium

loading or dedicated tritium loading experiments may be needed to estimate the bulk contribution.

According to the Frauenfelder solubility of H in W, tritium exposure at 300 K would prevent tritium to enter the bulk of the dust particles. According to the simulation presented here, 300 K exposure would lead to tritium sticking on the W surface. Thus, a tritium exposure at 300 K would only trigger the surface effects which could help to determine the contribution of the bulk contribution in the tritium loading experiment at higher temperature.

Isotopic exchange experiment at 300 K would also be a possible way to estimate the contribution of the bulk in the total activity. Indeed, room temperature isotopic exchange in the bulk of W is possible [35, 36] but only if the hydrogen isotopes are directly implanted in the bulk. Temperature above 473 K are required to do isotopic exchange in the bulk W with gas exposure [37, 38] as the solubility of H in bulk W is very low. Thus, isotopic exchange at 300 K after loading at 743 K could be a way to estimated the contribution of the bulk in the total tritium activity.

5.2. Coverage dependent desorption energies

Based on DFT calculations, we used coverage dependent desorption energies: in section 4, the tritium is easily recovered at low temperature because the desorption energy is lowered by the high coverage. Another way to describe this difference of desorption energies is to consider different adsorption sites with different desorption energies (from 1.4 eV to 0.8 eV for W(110) for instance). With such model, if there is no transfer between adsorption sites, it would not be possible to remove tritium trapped in the 1.4 eV sites at room temperature. However, such a picture deos not seems appropriate based on the isotopic exchange of H by D on W(100) performed by Tamm and Schmidt [26]. At 300 K, they observed a conversion of H by D, even on the desorption peak attributed to a site with a desorption energy of 1.4 eV.

5.3. Surface distribution

In section 3, the model suggests that the surface of the dust particles needs to be dominated by W(111) to reproduce the experimental data. The reason for that is not clear as W(110) surface is the most stable surface according to DFT calculations [39, 40]. A possible explanation could come from a competition between thermodynamics that favour the W(110) surface and the kinetic of defects on the surfaces that would favour the surface on which they moves the least. This process is used to explain the difference between square and spherical bcc iron nanoclusters depending on the condition (temperature and iron deposition) [41]: at low temperature and high iron deposition, (100) is favoured because of the high migration barrier of adatoms on (100) compared to (110). Similar to iron, the point defects on W surfaces, especially the adatoms, are more mobile on W(110) (≈1.0 eV) than on W(100) and W(111) (≈2.5 eV) [34]. Thus, depending on the temperature of formation of these dust particles, W(111) could be favoured over W(110). One has to note that we treat W micrometer size dust in this paper while the mechanism described in [41] is used on 10 nm iron clusters. This could vanish with the size and more studies are required which is not in the scope of this work. The other reason why W(111) seems dominant could also simply be that the various surface orientations of the dust have coverage dependent desorption energies similar to W(111).

5.4. Model for the sticking of hydrogen isotope molecules

In this model, the sticking rate of molecules from the gas phase to the surface is chosen to be proportional to $(1-\theta)^2$ based on the reaction involved in the sticking event. However, one could choose to change this model to have a linear dependence on $(1-\theta)$ (see Alnot [23]) or even no dependence at all. Changing toward such models speeds up the overall evolution of the hydrogen isotope coverage and the steady-state coverage. However, it does not have any impact on the tritium desorption calculated in figure 3 for the step (v). Indeed, during the quenching phase, the coverage reaches saturation and during step (iv) and (v) in figure 3, the tritium coverage is only driven by the desorption rate. It has to be pointed out that if the sticking rate is independent on the coverage, the coverage of W(100) and W(110) reaches more than 1 (or 1 if artificially blocked in the calculation) during the quench, even though the desorption energy (figure 2) is low for saturated surfaces.

In these simulations, we chose a sticking coefficient of H_2 independent of temperature and equal to 1 which seems to be an accurate value for clean metallic surfaces [22, 23, 12, 13]. However, if the surface is oxidised, the sticking coefficient may be reduced to a much lower value [9]. Indeed, pre-adsorption of O seems to affect the adsorption and desorption of H from W surface [42].

Concerning the simulation of the experimental results presented in section 3, the impact of the initial sticking coefficient, s_{T_2}, is assessed by varying it between 1 and 2×10^{-11} and doing the same optimisation as in section 3. The optimised tritium desorption curves are shown for the different values of s_{T_2} on figure 8(a). The value of the cost function $f_{c,2}$ for these optimised cases is given on figure 8(b) as a function of s_{T_2}. The tritium desorption curve

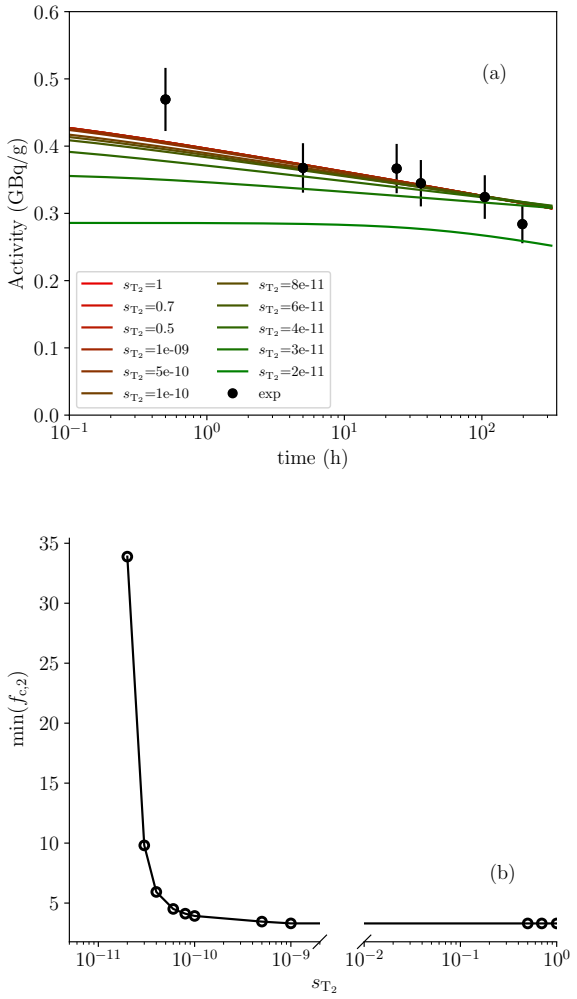

Figure 8: (a) Comparison between the experimental tritium activity and the simulated tritium activity for various values of the initial sticking coefficient. The simulated activities are the ones that give the minimum values of the cost function $f_{c,2}(P)$. These minimum values of the cost function are given in (b) as a function of the value of the sticking coefficient.

is independent of the sticking coefficient up to very low values down to 10^{-9} and it starts deviating significantly only for extremely low sticking coefficient (10^{-10}-10^{-11}). Such evolution is due to the quenching (phase (ii) and (iii) in figure 3) which freezes the desorption allowing accumulation of tritium on the surface. The deviation occurs when these two steps do not allow the tritium coverage to reach the initial coverage of step (v) obtained for $s_{T_2} = 1$. Thus, one should not use such an experiment (with high pressure) to assess the tritium sticking coefficient. It also means our assumption of a strong sticking coefficient does not impact the experimental validation of the model.

Considering the isotopic exchange, changing the initial sticking coefficient (for instance to 10^{-5}) would only modify the kinetics of tritium recovery (by a factor of 100,000). With a very efficient sticking, the kinetic of tritium loading is 10^{-7} seconds at 743 K and 10^5 Pa (figure 3 (a)). Thus a slower kinetic by a factor of 100,000 would not be problematic for a 2-hours-long tritium loading. However, the tritium recovery at 300 K or 373 K may be affected by such a change of kinetics if the dust particles are exposed to tritium for about an hour only.

Finally, the presence of adsorb oxygen atoms or oxides could modify the desorption energy. According to Whitten and Gomer, the pre-adsorbed oxygen tends to lower the desorption energy [42] which would fasten the desorption from the dust. But to follow the method presented on section 2.2, DFT data of H adsorption and desorption from oxidized W surfaces are required to consider such effects on the tritium sticking and desorption.

5.5. Effect of realistic pressure decrease

In section 4.2, we choose to simulate an increase and a decrease of the pressure of D_2 and T_2 in 5 seconds which represents a very rapid ramp down of the pressure. In a real tokamak, the pressure ramp down is limited by the pumping speed of the pumping system and the outgassing from the wall. The pressure decrease is expected to happen in the hundred seconds time scale for tokamaks with metallic walls like JET [43] or WEST [44].

Introducing a 100 seconds pressure ramp down instead of a 5 seconds one in the simulations does not change the outcome of the simulations: the tritium coverage increases during the pressure increase and quickly equilibrate after the pressure ramp down. However, the fact that the tritium pressure stays high increases the duration for which the tritium coverage is maximum. This has a negative effect on the control of the tritium inventory present in the tokamak vessel.

The impact of the slower ramp down goes in the opposite direction for the isotopic exchange situation which actually benefits from a lower pumping speed. Indeed, as shown in figure 7, the isotopic exchange stays efficient if the pressure of D_2 stays higher than the pressure of T_2. Thus, a slower ramp down keeps the deuterium pressure higher than the tritium one for a longer time enhancing the impact of the isotopic exchange.

6. Conclusions

In this work, we used a kinetic surface model to simulate tritium loading and desorption from micrometers-sized W dust. The desorption energies depends on

the hydrogen coverage of the W surface and are parametrised using density functional theory (DFT) data for W(110), W(100) [12] and W(111) [13]. This parametrisation allowed us to reproduce experimental desorption curve of tritium loading on $10\mu m$-sized dust particles that are relevant to the type of dust observed in WEST [7]. The experimental tritium desorption at 300 K could be reproduced by considering a linear combination of the tritium coverage on W(100), W(110) and W(111) with a predominance of W(111).

We also investigated the impact of the model on tritium uptake and removal from W surfaces in various scenarios. Exposure of dust particles to a mixture of deuterium and tritium gas can lead to dust with a massic activity of about 100 MBq/g for 10μm-sized dust. This tritium can be removed with isotopic exchange by exposing the dust either to H_2 or D_2 at low temperature (below 373 K) as soon as the tritium pressure is below the other isotopes. In particular, the kinetics of the isotopic exchange is much faster (below 20 seconds) than the natural room temperature desortpion (several hundreds of hours).

Appendices

A. Tritium activity of a batch of dust

We consider that each particle constituting a batch of powder can be approximated as a sphere of radius r. The volume and surface of one particle are:

$$S(r) = 4\pi r^2 \tag{16}$$

$$V(r) = \frac{4}{3}\pi r^3. \tag{17}$$

A batch of powder does not contain only one size of particles but rather a distribution characterised by a probability density function $f(r)$ (m^{-1}). We call $f(r)$ the number distribution as $f(r)dr$ gives the number fraction of particles having a radius between r and $r + dr$.

We consider that each particle of radius r is loaded with an equal quantity of tritium atom $N_T(r)$. Since one gram of tritium is equivalent to 360 TBq, it corresponds to a tritium activity $a_T(r)$ (Bq) of:

$$a_T(r) = \omega N_T(r) \tag{18}$$

where $\omega = 360 \times 10^{12} A_T/N_A$ is employed to convert a quantity of tritium atoms into a tritium activity, with $N_A = 6.022 \times 10^{23}$ mol^{-1} the Avogadro number and $A_T = 3$ g/mol the atomic mass of tritium. The contribution of each dust of radius r to the total activity a_{tot} (in Bq) is thus $a_T(r)f(r)dr$ and the total activity that can be measured is:

$$a_{tot} = \int_0^{+\infty} a_T(r)f(r)dr \tag{19}$$

The measured activity is usually normalised by the mass of the dust sample in order to have comparable quantities. The contribution of particles with a radius between r and $r + dr$ to the mass of the dust sample is $d_W V(r)f(r)dr$ with $d_W = 19.3 \times 10^6$ gm^{-3}. One gets the massic activity a_m (Bq/g) as:

$$a_m = \frac{\omega}{d_W} \frac{\int_0^{+\infty} N_T(r)f(r)dr}{\int_0^{+\infty} f(r)V(r)dr} \tag{20}$$

B. Calculating the tritium massic activity in the bulk from trap parameters

B.1. Concentration of interstitial tritium

Considering a piece of W exposed to a pressure p_{T_2} (in atm) of tritium at the temperature T, using the solubility measured by Frauenfelder [45], the concentration of interstitial (also called mobile) tritium c_m at the thermodynamic equilibrium is:

$$c_m = \rho_W 2.9 \times 10^{-5} \exp\left(-\frac{1.04 \text{ eV}}{k_B T}\right) \sqrt{p_{T_2}}. \tag{21}$$

where $\rho_W = 6.3 \times 10^{28}$ m^{-3} the W atomic density and p_{T_2} in Pa. For $T = 743$ K and $p_{T_2} = 1.1 \times 10^5$ Pa, we get $c_m = 8.3 \times 10^{-10}$ at.fr. which represents about 5 kBq/g. Calculation of tritium transport in W spherical particles with a radius of 7 μm shows that the tritium permeated from the surface to the centre of the sphere much faster (10 seconds) than the time scale of the experiment under the experimental exposure conditions (743 K, 1.1×10^5 Pa) . Thus, we assume the thermodynamic equilibrium is reached.

B.2. Effect of traps

Let's consider there are k traps with detrapping energies $E_{1 \leq i \leq k}$ and trap concentration $n_{1 \leq i \leq k}$. Based on the model described in [10, 11], the rate of detrapping is $\nu_i(T) = \nu_0 \exp\left(-E_i/k_B T\right)$ (with $\nu_0 = 10^{13}$ s^{-1} the pre-exponential factor of detrapping reaction) and the rate of the trapping is $\nu_m(T) = {}^{D(T)}/_{\lambda^2 n_{TIS}}$ with $D(T) = {}^{1.9 \times 10^{-7}}/_{\sqrt{3}} \exp\left(-{}^{0.2 \text{ eV}}/_{k_B T}\right)$ (m^{2}s^{-1}) the diffusion coefficient of tritium in W [33], $\lambda = 110$ pm the jumping distance for diffusion and $n_{TIS} = 6$ the number of tetrahedral interstitial site for H in W bcc lattice.

At the equilibrium between trapping and detrapping rate, for a given concentration of interstitial tritium, the quantity of tritium trapped in trap site i is [10, 11]:

$$c_{t,i} = \frac{n_i}{1 + \frac{\nu_i(T)}{\nu_m(T) c_m}} \tag{22}$$

and the total tritium concentration is $c_T = c_m + \sum_{1 \leq i \leq k} c_{t,i}$

B.3. Massic activity due to bulk tritium

B.3.1. case 1: intrinsic traps only In [32], simulations suggests there are 2 intrinsic traps in W: (0.87 eV, 10^{-3} at.fr.) and (1.00 eV, 4×10^{-4} at.fr.). Considering these intrinsic traps only, based on the equilibrium model described above, the corresponding tritium activity calculated with equation 1 is 0.027 MBq/g.

B.3.2. case 2: massic activity of 100 MBq/g with one trap If one measures a massic activity of about 100 MBq/g, the above equilibrium model suggests that it could correspond to a homogeneously distributed trap with a concentration of 10^{-3} at.fr. and a detrapping energy of 1.47 eV, or any couple (E, n) guaranteeing that $c_T = 1.54 \times 10^{-4}$ at.fr.. To increase the massic activity given by the equilibrium model, one need either to increase the detrapping energy to increase the fraction of filled trap (up to saturation) or increase the trap concentration.

References

[1] M. Shimada, R.A. Pitts, S. Ciattaglia, S. Carpentier, C.H. Choi, G. Dell Orco, T. Hirai, A. Kukushkin, S. Lisgo, J. Palmer, W. Shu, and E. Veshchev. In-vessel dust and tritium control strategy in iter. *Journal of Nuclear Materials*, 438:S996–S1000, 2013. Proceedings of the 20th International Conference on Plasma-Surface Interactions in Controlled Fusion Devices.

[2] Guido Mazzini, Tadas Kaliatka, and Maria Teresa Porfiri. Tritium and dust source term inventory evaluation issues in the european demo reactor concepts. *Fusion Engineering and Design*, 146:510–513, 2019. SI:SOFT-30.

[3] C. Grisolia, F. Gensdarmes, S. Peillon, G. Dougniaux, E. Bernard, A. Autricque, G. Pieters, B. Rousseau, S. Feuillastre, S. Garcia-Argote, O. Carvalho, V. Malard, I. George, L. Lebaron-Jacobs, T. Orsiere, C. Uboldi, J. Rose, M. Sanles Sobrido, D. Lambertin, D. Vrel, C. Decanis, K. Liger, T. Acsente, and G. Dinescu. Current investigations on tritiated dust and its impact on tokamak safety. *Nuclear Fusion*, 59(8):086061, jul 2019.

[4] A. El-Kharbachi, J. Chêne, S. Garcia-Argote, L. Marchetti, F. Martin, F. Miserque, D. Vrel, M. Redolfi, V. Malard, C. Grisolia, and B. Rousseau. Tritium absorption/desorption in iter-like tungsten particles. *International Journal of Hydrogen Energy*, 39(20):10525 – 10536, 2014.

[5] C. Grisolia, E. Hodille, J. Chene, S. Garcia-Argote, G. Pieters, A. El-Kharbachi, L. Marchetti, F. Martin, F. Miserque, D. Vrel, M. Redolfi, V. Malard, G. Dinescu, T. Acsente, F. Gensdarmes, S. Peillon, B. Pegourié, and B. Rousseau. Tritium absorption and desorption in iter relevant materials: comparative study of tungsten dust and massive samples. *Journal of Nuclear Materials*, 463:885 – 888, 2015. PLASMA-SURFACE INTERACTIONS 21.

[6] E Bernard, P Delaporte, F Jambon, B Rousseau, C Grisolia, D Chaudanson, and S Nitsche. Tungsten dust in fusion tokamaks: relevant dust laser production, characterization and behaviour under tritium loading. *Physica Scripta*, T167:014071, jan 2016.

[7] S. Peillon, G. Dougniaux, M. Payet, E. Bernard, G. Pieters, S. Feuillastre, S. Garcia-Argote, F. Gensdarmes, C. Arnas, F. Miserque, N. Herlin-Boime, C. Grisolia, and O. Pluchery. Dust sampling in west and tritium retention in tokamak-relevant tungsten particles. *Nuclear Materials and Energy*, 24:100781, 2020.

[8] Sabina Markelj, Olga V. Ogorodnikova, Primož Pelicon, Thomas Schwarz-Selinger, and Iztok Čadež. Temperature dependence of d atom adsorption on polycrystalline tungsten. *Applied Surface Science*, 282:478 – 486, 2013.

[9] M.A. Pick and K. Sonnenberg. A model for atomic hydrogen-metal interactions — application to recycling, recombination and permeation. *Journal of Nuclear Materials*, 131(2):208 – 220, 1985.

[10] E.A. Hodille, A. Založnik, S. Markelj, T. Schwarz-Selinger, C.S. Becquart, R. Bisson, and C. Grisolia. Simulations of atomic deuterium exposure in self-damaged tungsten. *Nuclear Fusion*, 57(5):056002, 2017.

[11] E.A. Hodille, S. Markelj, M. Pecovnik, M Ajmalghan, Z.A. Piazza, Y. Ferro, T. Schwarz-Selinger, and C. Grisolia. Kinetic model for hydrogen absorption in tungsten with coverage dependent surface mechanisms. *Nuclear Fusion*, 60(10):106011, sep 2020.

[12] M. Ajmalghan, Z.A. Piazza, E.A. Hodille, and Y. Ferro. Surface coverage dependent mechanisms for the absorption and desorption of hydrogen from the w(1 1 0) and w(1 0 0) surfaces: a density functional theory investiga-

tion. *Nuclear Fusion*, 59(10):106022, aug 2019.

[13] Z J Bergstrom, C Li, G D Samolyuk, B P Uberuaga, and B D Wirth. Hydrogen interactions with low-index surface orientations of tungsten. *Journal of Physics: Condensed Matter*, 31(25):255002, apr 2019.

[14] Jeffrey W. Bullard, Qingxu Jin, and Kenneth A. Snyder. How do specific surface area and particle size distribution change when granular media dissolve? *Chemical Engineering Journal*, 406:127098, 2021.

[15] Z.A. Piazza, M. Ajmalghan, Y. Ferro, and R.D. Kolasinski. Saturation of tungsten surfaces with hydrogen: A density functional theory study complemented by low energy ion scattering and direct recoil spectroscopy data. *Acta Materialia*, 145:388–398, 2018. cited By 2.

[16] Z A Piazza, M Ajmalghan, R D Kolasinski, and Y Ferro. A density functional theory based thermodynamic model of hydrogen coverage on the w(110) surface. *Physica Scripta*, T171:014025, jan 2020.

[17] P. W. Tamm and L. D. Schmidt. Binding states of hydrogen on tungsten. *The Journal of Chemical Physics*, 54(11):4775–4787, 1971.

[18] T.-U. Nahm and R. Gomer. The adsorption of hydrogen on w(110) and fe covered w(110) surfaces. *Surface Science*, 375(2):281 – 292, 1997.

[19] Eric Jones, Travis Oliphant, Pearu Peterson, et al. SciPy: Open source scientific tools for Python, 2001–. [Online; accessed 2018-08-10].

[20] Pauli Virtanen, Ralf Gommers, Travis E. Oliphant, Matt Haberland, Tyler Reddy, David Cournapeau, Evgeni Burovski, Pearu Peterson, Warren Weckesser, Jonathan Bright, Stéfan J. van der Walt, Matthew Brett, Joshua Wilson, K. Jarrod Millman, Nikolay Mayorov, Andrew R. J. Nelson, Eric Jones, Robert Kern, Eric Larson, C. J. Carey, İlhan Polat, Yu Feng, Eric W. Moore, Jake VanderPlas, Denis Laxalde, Josef Perktold, Robert Cimrman, Ian Henriksen, E. A. Quintero, Charles R. Harris, Anne M. Archibald, Antônio H. Ribeiro, Fabian Pedregosa, and Paul van Mulbregt. SciPy 1.0: fundamental algorithms for scientific computing in Python. *Nature Methods*, 17(3), March 2020.

[21] J. D. Hunter. Matplotlib: A 2d graphics environment. *Computing in Science & Engineering*, 9(3):90–95, 2007.

[22] Heather Bickley, James S Arlow, MA Morris, and David A King. Angle-integrated sticking probabilities: N2, h2 and d2 on w001. *Vacuum*, 31(10):507 – 509, 1981.

[23] P. Alnot, A. Cassuto, and D.A. King. Adsorption and desorption kinetics with no precursor trapping: Hydrogen and deuterium on w 100. *Surface Science*, 215(1):29 – 46, 1989.

[24] G. Federici, A.R. Raffray, and M.A. Abdou. Mistral: A comprehensive model for tritium transport in lithium-base ceramics: Part i: Theory and description of model capabilities. *Journal of Nuclear Materials*, 173(2):185 – 213, 1990.

[25] S. Markelj, A. Založnik, T. Schwarz-Selinger, O.V. Ogorodnikova, P. Vavpetič, P. Pelicon, and I. Čadež. In situ nra study of hydrogen isotope exchange in self-ion damaged tungsten exposed to neutral atoms. *Journal of Nuclear Materials*, 469:133 – 144, 2016.

[26] P. W. Tamm and L. D. Schmidt. Interaction of h2 with (100)w. ii. condensation. *The Journal of Chemical Physics*, 52(3):1150–1160, 1970.

[27] C. Grisolia. *Density control and plasma wall interaction in Tore Supra*, pages 1–8. Springer Netherlands, Dordrecht, 2000.

[28] J. Bucalossi, C. Brosset, D. Garnier, C. Grisolia, A. Grosman, G. Martin, and F. Saint Laurent. The conditioning procedures in tore supra after ciel implementation. *Journal of Nuclear Materials*, 313-316:263–268, 2003. Plasma-Surface Interactions in Controlled Fusion Devices 15.

[29] V. Rohde, R. Dux, A. Kallenbach, K. Krieger, and R. Neu. Wall conditioning in asdex upgrade. *Journal of Nuclear Materials*, 363-365:1369–1374, 2007. Plasma-Surface Interactions-17.

[30] D. Douai, S. Brezinsek, H.G. Esser, E. Joffrin, T. Keenan, S. Knipe, D. Kogut, P.J. Lomas, S. Marsen, I. Nunes, V. Philipps, R.A. Pitts, M. Shimada, and P. de Vries. Wall conditioning of jet with the iter-like wall. *Journal of Nuclear Materials*, 438:S1172–S1176, 2013. Proceedings of the 20th International Conference on Plasma-Surface Interactions in Controlled Fusion Devices.

[31] Z. Piazza, , R. Kolasinski, M. Ajmalghan, E. A. Hodille, and Y. Ferro. Hydrogen coverage on metal surfaces in the (μ, p, T) ensemble: A comparison of a thermodynamic model based on dft data for the (110) and (100) surfaces of tungsten with low energy ion beam analysis. *Accepted for publication in Journal of physical chemistry C*.

[32] E.A. Hodille, X. Bonnin, R. Bisson, T. Angot, C.S. Becquart, J.M. Layet, and C. Grisolia. Macroscopic rate equation modeling of trapping/detrapping of hydrogen isotopes in tungsten materials. *Journal of Nuclear Materials*, 467:424 – 431, 2015.

[33] N. Fernandez, Y. Ferro, and D. Kato. Hydrogen diffusion and vacancies formation in tungsten: Density functional theory calculations and statistical models. *Acta Materialia*, 94:307 – 318, 2015.

[34] Jiannan Hao, Shuo Jin, Guang-Hong Lu, and Haixuan Xu. Migration energy barriers and diffusion anisotropy of point defects on tungsten surfaces. *Computational Materials Science*, 184:109893, 2020.

[35] J. Roth, T. Schwarz-Selinger, V.Kh. Alimov, and E. Markina. Hydrogen isotope exchange in tungsten: Discussion as removal method for tritium. *Journal of Nuclear Materials*, 432(1):341 – 347, 2013.

[36] K. Schmid, U. von Toussaint, and T. Schwarz-Selinger. Transport of hydrogen in metals with occupancy dependent trap energies. *Journal of Applied Physics*, 116(13):134901, 2014.

[37] T. Ahlgren, P. Jalkanen, K. Mizohata, V. Tuboltsev, J. Räisänen, K. Heinola, and P. Tikkanen. Hydrogen isotope exchange in tungsten during annealing in hydrogen atmosphere. *Nuclear Fusion*, 59(2):026016, jan 2019.

[38] Tomi Vuoriheimo, Pasi Jalkanen, Anna Liski, Kenichiro Mizohata, Tommy Ahlgren, Kalle Heinola, and Jyrki Räisänen. Hydrogen isotope exchange mechanism in tungsten studied by ERDA. *Physica Scripta*, T171:014056, jan 2020.

[39] L. Vitos, A.V. Ruban, H.L. Skriver, and J. Kollár. The surface energy of metals. *Surface Science*, 411(1):186 – 202, 1998.

[40] J Byggmästar, M Nagel, K Albe, K O E Henriksson, and K Nordlund. Analytical interatomic bond-order potential for simulations of oxygen defects in iron. *Journal of Physics: Condensed Matter*, 31(21):215401, mar 2019.

[41] Junlei Zhao, Ekaterina Baibuz, Jerome Vernieres, Panagiotis Grammatikopoulos, Ville Jansson, Morten Nagel, Stephan Steinhauer, Mukhles Sowwan, Antti Kuronen, Kai Nordlund, and Flyura Djurabekova. Formation mechanism of fe nanocubes by magnetron sputtering inert gas condensation. *ACS Nano*, 10(4):4684–4694, 2016. PMID: 26962973.

[42] J.E Whitten and R Gomer. The coadsorption of h and o on the w(110) plane. *Surface Science*, 409(1):16 – 26, 1998.

[43] J. Denis, J. Bucalossi, G. Ciraolo, E.A. Hodille, B. Pégourié, H. Bufferand, C. Grisolia, T. Loarer, Y. Marandet, and E. Serre. Dynamic modelling of local fuel inventory and

desorption in the whole tokamak vacuum vessel for auto-consistent plasma-wall interaction simulations. *Nuclear Materials and Energy*, 19:550–557, 2019.

[44] R. Bisson, E.A. Hodille, J. Gaspar, D. Douai, T. Wauters, A. Gallo, J. Gunn, A. Hakola, T. Loarer, R. Nouailletas, J. Morales, B. Pégourié, C. Reux, R. Sabot, E. Tsitrone, S. Vartanian, E. Wang, N. Fedorczak, and S. Brezinsek. Deuterium and helium outgassing following plasma discharges in west: Delayed d outgassing during d-to-he changeover experiments studied with threshold ionization mass spectrometry. *Nuclear Materials and Energy*, 26:100885, 2021.

[45] R. Frauenfelder. Solution and diffusion of hydrogen in tungsten. *Journal of Vacuum Science and Technology*, 6(3):388–397, 1969.